JCTC Journal of Chemical Theory and Computation

ARTICLE

pubs.acs.org/JCTC

Rubredoxin Function: Redox Behavior from Electrostatics

Ana Patricia Gamiz-Hernandez,[†] Gernot Kieseritzky,[†] Hiroshi Ishikita,[‡] and E. W. Knapp*[,†]

[†]Institute of Chemistry and Biochemistry, Department of Biology, Chemistry and Pharmacy, Freie Universität Berlin, Fabeckstrasse 36a, D-14195, Berlin, Germany

[‡]Career-Path Promotion Unit for Young Life Scientists, Kyoto University, 202 Building E, Graduate School of Medicine, Yoshida-Konoe-cho, Sakyo-ku, Kyoto 606-8501, Japan

Supporting Information

ABSTRACT: Continuum electrostatic theory was applied to compute redox potentials of rubredoxin (Rd) proteins. We used multiple side chain conformers of Rd crystal structures, optimized geometries of salt bridges, mutated residues, and residues in the neighborhood of the iron−sulfur complex (FeS complex) self-consistently for given solvent pH and redox potential. The following contributions to Rd redox potentials are discussed: side chain conformations, H-bond geometries of the FeS complex, dielectric environment, charged residues, and salt bridges. We considered 15 different Rd's (of different species/strains and mutants) with available crystal structures whose redox potentials vary between −86 mV and +31 mV. The computed redox potentials deviated by less than 16 mV, root-mean-square deviation (RMSD), from measured values. The amide H-bond geometry is considered to be crucial for the variation of Rd redox potentials. To test this assumption, we considered 14 mutant Rd's for which we modeled the structures based on Rd from WT *Clostridium pasterianum (Cp)* leaving the amide H-bond geometry of the FeS complex invariant. Here, we obtained an RMSD of only 14 mV with measured values demonstrating that the amide H bond geometries cannot be a major factor determining Rd redox potentials. We analyzed the factors determining the Rd redox potentials of a mesophilic and a thermophilic Rd differing by nearly 90 mV. We found that half of the difference is due to sequence and half is due to backbone variations. Albeit salt-bridge networks vary considerably between these two Rd's and are considered to be responsible for differences in thermostability, their overall influence on Rd redox potentials is small.

INTRODUCTION

Iron−sulfur proteins are ubiquitous in living systems.[1−5] Rubredoxin (Rd) is a redox-active protein and belongs to the simplest type of iron−sulfur proteins. One of its functions is storing and transferring electrons to alkane hydroxylase from Rd reductase. Alkane hydroxylase belongs to a large class of membrane proteins of interest as biocatalysts for the production of alcohols, fatty acids, and epoxides.[6,7] The Rd's under study have 52 to 54 amino acids, except one with 45 residues. The redox-active iron sulfur complex (FeS complex) in Rd consists of a single iron, ligated to four sulfur atoms of cysteine residues (see Figure 1). The FeS complex in Rd involves only a single iron. Thus, quantum chemical computations are facilitated considerably, since antiferromagnetic coupling appearing in multinuclear FeS complexes is absent.[8−14] Studies on iron sulfur proteins and corresponding model systems have demonstrated that several factors are important in understanding their redox properties.[3,5,9−13,15−25] These are the number, types, and strengths of H bonds with the FeS complex;[3,5,13,15,17,21−25] the polarity and protonation states of residues surrounding the FeS complex;[26,27] the degree of solvent exposure;[16,20,21,28] and quite generally, the electrostatic environment defined by the protein−solvent boundary.[9−12,20]

Using NMR spectroscopy, Lin et al.[15,23] found a correlation between the redox potentials of Rd's from *Clostridium pasterianum* (*Cp*) mutants and the strengths of the six amide H bonds with the FeS complex characterized by H-bond lengths. They inferred variations of H−S distances ranging from 2.2 Å to 2.8 Å and concluded that these are essentially responsible for the variations of redox potentials of different Rd's from mutant *Cp*.

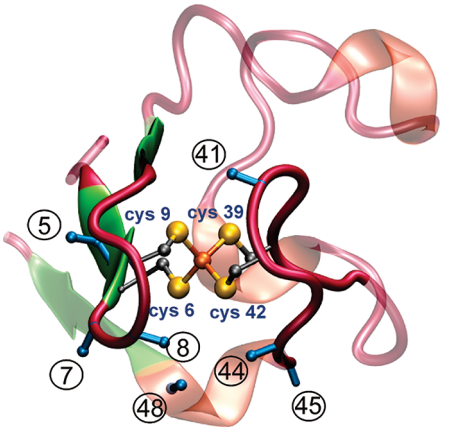

Figure 1. Rubredoxin (Rd) crystal structure from *Cp* (PDB code 1IRO[38]) with 53 amino acids and the iron−sulfur complex (FeS complex) in the center. The iron is covalently bound to four cysteine sulfur atoms belonging to two different protein loops (in red). Blue $C_\alpha-C_\beta$ bonds with residue numbers depict amino acid side chains of Rd that can have an impact on the redox potential, as will be discussed in text.

Received: August 24, 2010
Published: January 21, 2011

Table 1. Sequence Comparison between Eight Rubredoxins (Rd) from Seven Different Species (Two Different Strains from *Dv*) with Available Crystal Structures: *Clostridium Pasterianum* (*Cp*),[38,81] *Desulfovibrio Desulfuricans* (*Dd*),[82,83] *Desulfovibrio Gigas* (*Dg*),[84,85] *Desulfovibirio vulgaris* (*Dv*),[86−88] *Pyrococcus Abbyssi* (*Pa*),[25,80] *Pyrococcus Furiosus* (*Pf*),[32,49,89] and *Pseudomonas aeruginosa* (*Ps*)[7] [a]

Rd	1									11										21										31										41										51
Cp	M	K	K	Y	T	C	T	V	C	G	Y	I	Y	N	P	E	D	G	D	P	D	N	G	V	N	P	G	T	D	F	K	D	I	P	D	W	V	C	P	L	C	G	V	G	K	D	Q	F	E	E	V	E	E
Pf[3]	-	A	K	W	V	C	K	I	C	G	Y	I	Y	D	E	D	A	G	D	P	D	N	G	I	S	P	G	T	K	F	E	E	L	P	D	D	W	V	C	P	I	C	G	A	P	K	S	E	F	E	K	L	E	D
Dg	M	D	I	Y	V	C	T	V	C	G	Y	E	Y	D	P	A	K	G	D	P	D	S	G	I	K	P	G	T	K	F	E	D	L	P	D	D	W	A	C	P	V	C	G	A	S	K	D	A	F	E	K	Q		
Dd	M	Q	K	Y	V	C	N	V	C	G	Y	E	Y	D	P	A	E	H	D																	N	V	P	F	D	Q	L	P	D	D	W	C	C	P	V	C	G	V	S	K	D	Q	F	S	P	A
Dv[1]	M	K	K	Y	V	C	T	V	C	G	Y	E	Y	D	P	A	E	G	D	P	D	N	G	V	K	P	G	T	A	F	E	D	V	P	A	D	W	V	C	P	I	C	G	A	P	K	S	E	F	E	P	A		
Dv[2]	M	K	K	Y	V	C	T	V	C	G	Y	E	Y	D	P	A	E	G	D	P	D	N	G	V	K	P	G	T	S	F	D	D	L	P	A	D	W	V	C	P	V	C	G	A	P	K	S	E	F	E	A	A		
Pa[4]	M	A	K	W	R	C	K	I	C	G	Y	I	Y	D	E	D	E	G	D	P	D	N	G	I	S	P	G	T	K	F	E	D	L	P	D	D	W	V	C	P	L	C	G	A	P	K	S	E	F	E	R	I	E	
Ps	M	R	K	W	Q	C	V	V	C	G	F	I	Y	D	E	A	L	G	L	P	E	E	G	I	P	A	G	T	R	W	E	D	I	P	A	D	W	V	C	P	D	C	G	V	G	K	I	D	F	E	M	I	E	

[a] Some of the conserved residues are highlighted in different background colors: cysteines in yellow, amino acids surrounding the FeS complex (see Fig. 1) in light gray, amino acids belonging to different salt-bridge patterns in the crystal structures in dark blue/red/green (see details in Supporting Information Table S3). The residue numbers in the first line refer to Rd from *Cp*. [1] Miyazaki strain of *Dv*. [2] Hildenborough strain of *Dv*. [3] N-terminal alanine forms a salt bridge with D14. [4] In *Pa*, E53 is involved in two different salt bridges: a side chain of E53 with K3 and C-terminal acidic group of E53 with R51.

However, the mutations of Rd do not only vary the H-bond strengths but also conformations, charge distributions, and the electrostatic boundary between the protein and solvent, which all can shift the Rd redox potentials.[20,21,29] One purpose of the present work is to study the influences of these different factors on Rd redox potentials.

Subtle conformational details may also influence the redox potentials of Rd-like FeS complexes.[30] In this context, it is worth mentioning that the FeS complex structures of Rd's vary with the redox state[31−34] and differ from crystal structures of small Rd-like FeS-complex models.[21,35] Such conformational changes of Rd-like FeS complexes are quite important, as steric constraints imposed by the protein alter the geometry and energetics.[21,35] Therefore, quantum chemical computations of small FeS complexes may not faithfully describe the properties of the FeS complex in the protein, while larger models[36] that can represent the protein environment more faithfully may introduce new problems, if they possess several energy minima with different geometries.[37]

One of the challenges of the Rd function is to understand that at room temperature (T = 25 °C) the redox potential from the mesophilic *Cp* is at −55 mV, while it is at +31 mV[39] from the thermophilic *Pyrococcus furiosus* (*Pf*)[39] species, albeit the structures (backbone RMSD of about 0.5 Å) and sequences (sequence similarity of 70%, sequence identity close to 60%, see Table 1) are similar. The sequences of Rd's from these two species vary in charged residues and salt bridges, which were suggested to play a role in thermostability.[40−42] Surprisingly, the Rd redox potential from WT *Pf*, which at room temperature is +31 mV, assumes a value of −93 mV at 95 °C,[39] much lower and close to the room temperature value of −77 mV of Rd from WT *Cp*. Understanding the peculiarities of redox potentials of these two Rd's has been the subject of many experimental and theoretical studies during recent years.[16,27,29,32,39,43−57]

Two main sources for temperature dependent redox potentials of proteins can be named. (i) One reason for the observed downshift of the Rd redox potential with rising temperature could be the lowering of the water dielectric constant at higher temperatures,[39] which at T = 100 °C is as low as ε_w = 55.5.[58] Assuming that the thermophilic Rd structure remains invariant at high temperatures, the FeS complex does not become solvent exposed, such that there is only a moderate decrease in dielectric screening of the FeS complex. This may destabilize the more negatively charged reduced state (total charge −2) slightly more than the oxidized state (total charge −1). Hence, we would expect a small downshift of the Rd redox potential with rising temperature. This is likely the result of subtle changes in the protonation pattern that can also influence the Rd redox potentials. (ii) A second source is certainly structural changes induced at higher temperatures. Partial unfolding of the very stable Rd from the thermophilic species *Pf* is unlikely. Opening of small cavities close to the FeS complex could allow water to penetrate and form additional H bonds with the negatively charged sulfurs of the FeS complex. Again, this would stabilize more the reduced than the oxidized state and thus upshift the redox potential with rising temperature, opposite to the trend observed in experiments. However, the six amide H bonds with the sulfurs of the FeS complex may become loose at higher temperatures. This would destabilize the reduced state more than the oxidized state, resulting in a potentially significant redox potential downshift, as observed in experiments. Albeit these temperature effects are certainly of interest, we restrict our present study to room temperature only.

To compute the Rd redox potentials, we evaluate electrostatic energies in continuum dielectric models.[59−69] This procedure yielded agreement with experiments for protein cofactors as different as hemes,[62,63,66,69] chlorophylls,[68] and quinones[64,65,67] in different types of proteins. In this approach, measured redox potentials of appropriate model systems in solvents were used as references to compute the shift in redox potentials between the solvent and protein environment, evaluating the electrostatic energies of solvation. For Rd-like FeS complexes, such experimental redox potential values are not available. Therefore, we considered in a previous study[21] FeS complex model compounds whose redox potentials were obtained by a combination of *ab initio* quantum chemical and electrostatic energy computations. This study is in line with previous work[21,70,71] where we computed redox potentials of a larger number of organic compounds[70] and transition metal complexes,[71] yielding agreement with experimental results with a root-mean-square deviation (RMSD) of 55 mV and 60 mV, respectively. For a small Rd-like FeS complex, $[Fe(SCH_2CH_3)_4]^{-,2-}$ with S_4 instead of the

C_2 symmetry prevalent in Rd our computations yielded in acetonitrile a redox potential of −813 mV, as compared to the measured value of −838 mV.[71] Using the same approach, we obtained for a large Rd-like FeS complex[21] that mimics the situation in Rd faithfully with proper C_2 symmetry and H-bond pattern a redox potential of +194 mV in a dielectric continuum of ε_w = 80 corresponding to water. In the present work, we considered the complete Rd protein from different species and from different mutants to study the variation of the redox potentials of the embedded FeS complex. These Rd redox potentials were computed with the newly developed extended version of the program Karlsberg+.[72,73] In contrast to the former version of Karlsberg,[61] which uses the charge model of a single protein structure (closely related to a corresponding crystal structure with optimized hydrogen atom positions), the new Karlsberg version can be used to compute pK_A values and redox potentials in proteins by optimizing not only hydrogen atom positions but also specific amino acid side chains self-consistently at a given solvent pH and redox potential.

The aim of this study is to understand how Rd proteins from different species tune their FeS complex redox potentials by varying the amino acid composition and protein conformation. We quantify how much the dielectric environment affects the redox potentials of different Rd's from mutant *Cp* by modeling the Rd structures using a polypeptide backbone and unchanged side chain conformers from the WT *Cp* crystal structure. Since the amide H bonds with the FeS complex remain invariant in these mutant Rd structures, we can study redox potential variations of factors that differ from H-bond strengths. We also investigated the role of charged amino acids and salt bridges to understand the redox potential differences between mesophilic and thermophilic Rd's. Furthermore, we consider the conformational variations observed in Rd crystal structures and evaluate the influence they have on Rd redox potentials.

METHODS

Foundations and Conditions for Electrostatic Energy Computations. All redox potentials reported in this work are based on electrostatic energies evaluated by solving numerically the linearized Poisson−Boltzmann equation:

$$\vec{\nabla}\bullet[\varepsilon(\vec{r})\vec{\nabla}\phi(\vec{r})] - \kappa^2(\vec{r})\,\phi(\vec{r}) = -4\pi\rho(\vec{r}) \qquad (1)$$

using the program APBS[74,75] to obtain the electrostatic potential ϕ, where ε is the dielectric constant, κ is the ionic strength, and ρ is the charge distribution. The total electrostatic energy is given by refs 60 and 72:

$$\Delta G^{(n,l)} = \sum_{\mu=1}^{N} x_\mu^{(n,l)}(g_\mu^{(l)} - g_{\mathrm{ext},\mu}) + \sum_{\mu,\nu=1,\mu<\nu}^{N} x_\mu^{(n,l)} x_\nu^{(n,l)} \Delta\Delta w_{\mu\nu}^{(l)} + \Delta G_{\mathrm{conf}}^{(l)} \qquad (2)$$

where μ and ν label the total number of N-charge variable (titratable or redox-active) groups in the protein, while n labels one of the many possible combined protonation/redox patterns and l labels the protein conformer. The zero point of energy corresponds to the reference charge state where all titratable groups are deprotonated and all redox-active groups are reduced. The set of integers $x_\mu^{(n,1)}$, μ = 1, ...N, describes the protonation/redox pattern n in protein conformer l; $x_\mu^{(n,1)}$ vanishes if the group μ is deprotonated/reduced and is unity if the group μ is protonated/oxidized. The first term in eq 2 considers the electrostatic energy of individual charge variable groups μ in protein conformer l, if all other charge variable groups $(\nu: \nu \neq \mu)$ are in the reference charge state. The second term in eq 2 considers the correction energy necessary, if the other charge variable groups (ν) are not in the reference charge state where $x_\nu^{(n,1)} = 0$. The third term in eq 2 accounts for the specific protein conformer l and vanishes if the reference conformer is adopted. The reference conformer can be arbitrarily chosen and in principle also the reference charge state, defining thus the zero point of energy of $\Delta G^{(n,l)}$. However, in the latter case, the $x_\mu^{(n,1)}$ in eq 2 have to be replaced by $\Delta x_\mu^{(n,1)} = x_\mu^{(n,1)} - x_{\mu,\mathrm{ref}}^{(n,1)}$, where the $x_{\mu,\mathrm{ref}}^{(n,1)}$ characterize the reference charge state. Since the energy eq 2 is only applied to evaluate energy differences, the choice of reference state has no influence on the results. The free energy of a proton or electron in the solvent is given by $g_{\mathrm{ext},\mu}$, where the index μ is only needed to discriminate between the proton and electron depending on the type of charge variable group μ. If μ is a titratable group, $g_\mu^{(1)} = -\ln(10)\,RT_{298K}\mathrm{p}K_{A,\mathrm{intr},\mu}^{(1)}$ and $g_{\mathrm{ext},\mu} = -\ln(10)\,RT_{298K}$ pH. If μ is a redox-active group, $g_\mu^{(1)} = F\cdot e_\mu^{(1)}$ and $g_{\mathrm{ext},\mu} = F\cdot e_{\mathrm{solv}}$, where F is the Faraday constant and $e_\mu^{(1)}$ and e_{solv} are the redox potentials of redox-active group μ and the solvent, respectively. How the energy terms $g_\mu^{(1)}$ and $\Delta\Delta w_{\mu\nu}^{(1)}$ from eq 2 are evaluated with the help of the PB eq 1 is explained in detail in refs 60 and 72. The probability of the charge variable group μ to be in its protonated/oxidized state is computed as a Boltzmann average:

$$\langle x_\mu \rangle = \frac{1}{Z}\sum_{n,l} x_\mu^{(n,l)} \exp\left(-\frac{\Delta G^{(n,l)}}{RT}\right) \text{ with } Z = \sum_{n,l} \exp\left(-\frac{\Delta G^{(n,l)}}{RT}\right) \qquad (3)$$

where the sums in eq 3 run over all conformers (l) and charge states (n). Since the number of different charge states can be enormously large, the sums are evaluated using Metropolis Monte Carlo importance sampling, as explained in more detail in ref 61.

The protein was described as a set of atomic partial charges [defining thus the charge distribution $\rho(\vec{r})$ in the PB eq 1] embedded in an inhomogeneous dielectric continuum where the dielectric constant was set to ε_p = 4 inside the protein and ε_w = 80 outside for bulk water. The more details of the protein are modeled explicitly, the lower is the value of the dielectric constant inside the protein volume. Considering a single or few protein conformations with a detailed atomic charge model and flexible protonation pattern, as done in the present study and in a legacy of our past studies, the dielectric constant ε_p = 4 accounting for electronic polarizability and residual conformational variation of amino acid side chains of the protein yielded the best results. Larger values of the dielectric constant ε_p would become necessary if the protein model was less detailed. This is, for instance, the case for the aqueous solvent, where ε_w = 80 is used, since no molecular details are considered. If two different electrostatic models of the same protein yield the same quality of agreement, the model with the lower value of the dielectric

constant is superior. Since one reviewer was questioning the dependence of the computed redox potentials on the protein dielectric constant, we added results for $\varepsilon_p = 2$ and 8, which are discussed later, together with the results on the Rd mutants from *Cp*, and presented in detail in Figure S1 in the Supporting Information.

The boundary interface between the protein and solvent lumen was calculated by the molecular surface routine implemented in APBS using a solvent probe radius of 1.4 Å. Large enough cavities inside the protein can also be detected by this algorithm, such that inside their volumes a dielectric constant of $\varepsilon_w = 80$ can be assigned. This feature becomes relevant if one considers mutants where a voluminous side chain is replaced by a smaller one. An ionic strength of potassium chloride concentration at 100 mM was implicitly included.

An alternative approach would be to use explicit water and to evaluate the energetics of the different protonation and redox pattern by molecular dynamics (MD) simulations, as done by other groups.[76,77] This protein−water model is more detailed but requires ensemble averaging over different water conformations. The amount of CPU time needed when generating by MD simulations the necessary number of water conformations for a single combined protonation and redox pattern may be roughly the same as the time needed to solve a single linearized PB equation. However, MD simulations must be performed for each protonation pattern. In contrast, due to the additivity of electrostatic energies obtained by the linearized PB equation, it can be solved independently for the states of the individual titratable and redox-active groups. Hence, for a protein like Rd from WT *Cp*, with 20 titratable residues, 2^{20} MD simulations are necessary, while in the present approach the PB equation needs to be solved roughly only 2×20 times. The typical accuracy for pK_A computations is about 1 pK_A unit corresponding to 60 meV.[72] For redox potential computations, we expect an even higher accuracy, since changes of the charge pattern between the different states of a redox-active group are less localized than for protonation changes of titratable groups.

Atomic Partial Charges and Redox Potential of the Reference FeS Complex. Atomic partial charges were taken from the CHARMM22 force field[78,79] if available. For the FeS complex, atomic partial charges were adapted from previous work where electrostatic potentials were computed with a combination of quantum chemical and electrostatic methods applied to the small Rd-like model $[Fe(SCH_2CH_3)_4]^{-,2-}$ in C_2 symmetry,[21] yielding a redox potential value of +56 mV in water (ε = 80) and −165 mV for a continuum dielectric medium, corresponding approximately to protein environment (ε = 20, Table 3 in ref 21). The too low value of the redox potential in the latter case is due to the absence of explicit H bonds with the sulfur atoms of the FeS complex in this small Rd-like model. The charge model of a more realistic larger Rd-like FeS complex involving C_2 symmetry and the appropriate H-bond pattern (model 4 in ref 21 with six amide H bonds), as it appears in Rd, yielded a redox potential value in water of +194 mV. The same large model embedded in a continuum dielectric of ε = 20 that roughly approximates the protein environment, if for the protein no explicit atomic charges are used, yielded +57 mV,[21] which is close to the interval (−87 to +39 mV) of measured Rd redox potentials. However, this large Rd-like model is too complex and in conflict with the CHARMM charge model and cannot easily be adjusted to compute electrostatic energies considering a detailed protein model with atomic charges. Therefore, we used in the present study the smaller reference model $[Fe(SCH_2)_4]^{-,2-}$ whose charges were made compatible with the CHARMM force field. For this smaller model, no measured redox potentials are available, presumably since it is not stable in solution. A detailed explanation is given in section S1 and charges are listed in Table S2 of the Supporting Information. Alternatively, using a reference redox potential value of +112 mV (56 mV larger than the redox potential computed for the small Rd-like model in a dielectric medium of ε = 80) for the small charge adapted FeS complex in water ($[Fe(SCH_2)_4]^{-,2-}$), the RMSD between computed and measured Rd redox potentials is minimized (see section S2 in the Supporting Information for a detailed discussion). The differences of the computed redox potentials with this reference redox potential are within the range of deviations to be expected from the *ab initio* computational method employed[21,70,71] for the Rd-like FeS complexes. Since the variations in measured Rd redox potentials to be analyzed are of the same size as these differences, we prefer to use +112 mV as a reference redox potential value for the small FeS complex in our computations. Thus, we have introduced an adjustable parameter in the electrostatic energy computations.

Redox Potential Computations in Proteins with Multiconformers. For the electrostatic computations of the Rd redox potentials, we employed a modified new version of Karlsberg+,[72,73] which we used in the past primarily for accurate pK_A computations. Karlsberg+ combines classical electrostatic energy computations with pH-dependent conformational relaxation of salt bridges and H bonds inside proteins. The original Karlsberg+, available on the Web, tries to predict alternative atom positions for side chains of basic and acidic residues involved in salt bridges under high and low pH conditions, where these salt bridges are generally not stable any more. It does so by generating pH adapted conformations (PACs) that are obtained by self-consistent geometry optimizations of the input crystal structure combined with random changes of side chains of basic and acidic residues. In the new modified version of Karlsberg+, we consider redox rather than pH-dependent alternative side chain conformers. Accordingly, we introduced redox and pH 7 adapted conformations (RACs) for a given Rd redox state in the same spirit as we introduced PACs before to describe the pH dependence of the protonation pattern.[72] These RACs can also be generated to model side chain conformers of mutated residues. FeS complex redox potential contributions due to specific amino acids were analyzed by setting the charges of the corresponding side chain atoms to zero while computing the Rd redox potential.

Generating Redox Potential Adapted Conformers (RACs). To compute redox and protonation equilibria in proteins, solvent pH and solvent redox adapted equilibrium protein conformers are generated from the appropriate crystal structures where hydrogen atoms were added by Karlsberg+. In summary, Karlsberg+ consists of three modules: (i) generation of PACs or RACs using a special CHARMM[78] script, (ii) computation of electrostatic energies with the Poisson−Boltzmann solver APBS,[74,75] and (iii) Boltzmann averages of protonation and redox patterns and conformations (inherent in PACs or RACs) using the Metropolis Monte Carlo algorithm as in our legacy program Karlsberg.

This task is solved by self-consistent geometry optimization determining the most likely occupied protein conformations (with respect to protonation and redox pattern, hydrogen atoms, and side chain conformers of a selected set of residues) without

knowing its most likely protonation pattern and vice versa. To achieve this goal, Karlsberg+ performs an iterative procedure analogous to quantum mechanical self-consistent energy computations. First, Karlsberg+ calculates an initial protein protonation pattern at a high dielectric constant of $\varepsilon_p = 80$ everywhere (to avoid an unphysical protonation pattern, which may easily appear initially) by adding and optimizing hydrogen atoms in the crystal structure with standard protonation (acids deprotonated and bases protonated). On the basis of this first guess of protonation pattern, Karlsberg+ performs geometry optimizations (at ambient pH and a given redox state using the CHARMM22[78] force field with $\varepsilon_p = 1$ everywhere for all iteration steps) of amino acid side chains (including hydrogens) involved in salt-bridges and a selection of others that may influence the cofactor redox potential starting with a set of 30 structures with randomized side chain geometries for the considered amino acids. The resulting lowest energy global conformer of the protein is used in the next step to re-evaluate the protonation pattern by electrostatic energy computations (from now on, with $\varepsilon_p = 4$ in the protein and $\varepsilon_w = 80$ outside). If it changes, the geometry optimization step is repeated using the new protonation pattern. The cycle is repeated until the protonation pattern remains constant at a given pH and redox state. With this procedure, five RACs are generated for each redox state at ambient pH, starting with a different random seed in each case. Finally, Karlsberg+ computes redox titration curves of the protein using the ensemble of generated RACs with their electrostatic energies. This is done using Metropolis Monte Carlo importance sampling according to eq 3 considering the states of lowest electrostatic energy of the protonation, redox, and conformation pattern of the protein and allows calculating the redox potentials as proper Boltzmann-weighted thermodynamic averages.[61]

Besides the treatment of salt bridges, Karlsberg+ can now also generate RACs with geometry optimized side chains of mutated residues (and of other electrostatically relevant side chains of varying geometry), which is useful when no experimental coordinates are available for them. Since the side chains of the mutated residues possess different volumes and shapes than the side chains they are replacing, we included also the side chains of the neighbor residues (around 4 Å from the mutated residue) in the optimization procedure to generate RACs. If, for the same protein, crystal structures from two different species are available, it is instructive to build RACs that use the whole polypeptide backbone and chain conformers of all conserved residues from one protein but have inserted side chain conformers of the other protein structure for the nonconserved residues. In case side chains were found in multiple conformations in the protein crystal structure, RACs were generated for each combination of side chain conformers and used in the Boltzmann averaging.

Relaxing amino acid side chains can also be quite useful, if a protein crystal structure involves structural deficiencies. This is for instance the case for Rd crystal structures from *Cp* that were solved as trimers[28,55] and tetramers,[80] where some side chains belonging to different monomers are in too close contact and needed to be relaxed.

Usage of Rubredoxin Crystal Structures and RACs. The experimental information of atomic coordinates of all considered Rd's in this study were taken from the protein database (PDB): these are the WT structures of Rd's in the oxidized state from eight different species/strains, as listed in Table 1, where the sequences are aligned. We also considered available Rd crystal structures in the reduced state from *Cp* (WT[31] and L41A mutant[34]) and from WT *Pf*.[32] The lengths of the six amide H bonds with the sulfur atoms of the FeS complex vary within the same Rd and between different Rd's typically between 3.34 and 3.99 Å, with an average of about 3.5 Å (see in ref 21 Supporting Information Table S1.2). More information regarding PDB codes, structure resolutions, redox states, and the literature are given in Table S3 of the Supporting Information.

We also used crystal structures of Rd's from mutant *Cp* (l41A,[34] V44L,[55] V44A,[55] V44G,[55] and V44G/G45P[55]) and from mutant *Pa* (W4L/R5S and W4L/R5S/A44S[25,80]). We excluded Rd structures based on NMR experiments. All Rd crystal structures from *Cp* (WT and mutants) were pairwise superimposed using the Kabsch algorithm[90] relative to the structure from WT *Cp* (1FHH) considering atoms of the FeS complex only (iron, sulfurs, and C_β atoms of the four ligating cysteines) to detect residues whose side chains are in different conformation (see Supporting Information Table S4). In four Rd crystal structures (WT *Cp* and V44A, V44G, and V44L mutant *Cp*), coordinates of the C-terminal residue (E54) are missing (53C_α−Fe distance 18.2 Å). The missing atoms were modeled yielding computed redox potentials that deviated by less than 4 mV from the corresponding values in absence of E54. Therefore, in the following, computed redox potentials of these Rd's refer to the crystal structures without a modeled C-terminal residue.

We computed the Rd redox potentials using two different sets of RACs generated by Karlsberg+: a minimal and an extended set. In the minimal set of RACs, we considered all available crystal structure data. These are crystal structures from different laboratories, for different redox states, for all monomers, if there are several monomers per unit cell and for all combinations of multiple side chain conformers (for more details, see Supporting Information Table S3). For the three Rd's, where crystal structures are available for both redox states, we generated RACs of the oxidized state also using the reduced crystal structure and vice versa. The RACs for the extended set are obtained by generating for each RAC of the minimal set all combinations of side chain geometries (1) of residues involved in salt-bridges, (2) of selected residues near the FeS complex, and (3) of mutated residues (if no corresponding crystal structures are used instead). All generated RACs were generated at constant pH = 7. Note that RACs based on a single Rd crystal structure involve only side chain and no backbone variations. However, we also used different Rd crystal structures (from different laboratories, for different redox states, different monomers in the unit cell of the same crystal) and generated for each of these structures RACs. Hence, the complete set of RACs involved also backbone variations if not otherwise stated.

Measured Rd Redox Potentials. Measured redox potentials of all considered Rd's are listed in Table S5 (Supporting Information). Redox potentials of the same protein measured by different groups vary by about 20 mV. This may be due to different measurement methods and usage of redox modifiers (like polylysine) to obtain stable square voltammetry for negatively charged proteins like Rd.[29,91] The use of these modifiers can slightly upshift redox potentials.[29,91] Furthermore, there are small variations of pH and temperature where Rd redox potentials were measured (see for example Rd from *Pf*, Table S5). Accordingly, Rd redox potentials are more positive at lower than at higher pH[92] and decrease with higher temperatures.[39] In our redox potential computations, we assume standard conditions,

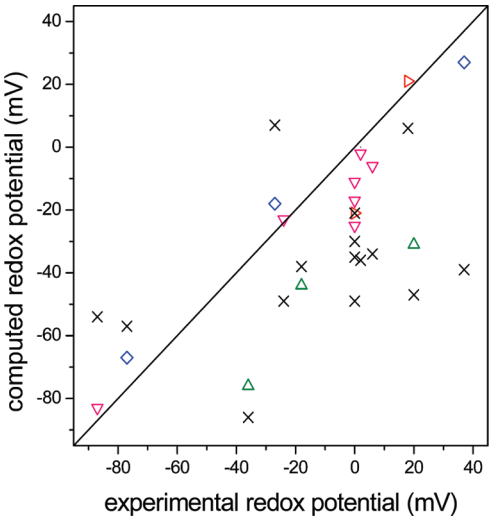

Figure 2. Comparison of measured and computed redox potentials of Rd's with 15 different sequences using the corresponding crystal structures. These are WT Rd's from eight different species/strains (*Cp*, *Pa*, *Pf*, *Ps*, *Dg*, *Dv*(H), *Dv*(M), and *Dd*) and seven Rd's from mutant *Cp* (V44A, V44L, V44A/G45P, V44G, and L41A) and from mutant *Pa* (W4L/R5S and W4L/R5S/A44S). The symbol "×" refers to computations based on the minimal set of RACs (see Methods, RMSD 42 mV). The open symbols (blue ◇, red right-facing △, green △, and magenta ▽) refer to computations using the larger extended set of RACs (RMSD 16 mV). For the 12 Rd's marked by open triangles (red right-facing △, green △, and magenta ▽), crystal structures are only available for the oxidized states. For the three Rd's marked by blue ◇, crystal structures are also available for the reduced states. The three Rd redox potentials from *Pa* denoted by green △ were measured in the same lab[80] using polylysine as a redox modifier that can upshift Rd redox potentials (see discussion in text). Rd redox potential values from two species (*Cp* V44A/G45P and WT *Ps*) denoted by red right-facing △ were not measured but estimated.[7] Redox potentials are listed in Table S7 (Supporting Information).

i.e., pH 7 and 25 °C, and no adjustment of measured redox potentials due to the use of redox modifiers was considered.

RESULTS AND DISCUSSIONS

Overview of Computations. The evaluation of Rd redox potentials in this study consists of five parts. (1) Rd redox potentials of different species and their mutants were computed using the minimal set of RACs as described in the Methods section and Table S3 (Supporting Information). (2) We considered the same Rd's but use now the extended set of RACs as described in the Methods section. (3) To study the dependence of the Rd redox potentials on H-bond geometries, side chain conformers, and charges, we focused on mutant Rd's from a single species (*Cp*), using RACs that were based on the single Rd crystal structure from WT *Cp*. (4) We consider the Rd's from mesophilic *Cp* and thermophilic *Pf* to discuss the factors that explain the difference in their Rd redox potentials. (5) The protein backbone variation close to the FeS complex observed in Rd crystal structures from *Pa* (mutant W4L-R5S) allows for studying computationally how geometry variations of H bonds with FeS complex sulfurs influence the Rd redox potential.

1. Computed Rd Redox Potentials Based on the Minimal Set of RACs. We generated RACs according to the minimal set. In these preliminary computations, the correlation between measured and computed Rd redox potentials is poor (RMSD of 42 mV; see "×" in Figure 2; values are listed in Supporting Information Table S7). Results of similar quality were reported before[16] using solely Rd crystal structures, optimizing only hydrogen atom positions. Some improvement was obtained when the computed Rd redox potentials were based on structures from MD simulations[16,57] However, these MD based approaches generally involve global changes in Rd structures, making it difficult to quantify the different redox potential contributions. In the present study, only moderate structural modifications of the Rd crystal structures were considered, making it easier to identify specific influences on Rd redox potentials, as shown in the next two sections, 2 and 3.

2. Computed Rd Redox Potentials Based on the Extended Larger Set of RACs. We calculated the Rd redox potentials again using the extended larger set of RACs. Here, we optimized side chains of a selected set of residues close to the FeS complex (5, 7, 8, 41, 44; see Figure 1) and of residues involved in salt bridges for the oxidized and reduced states. In studies of Rd's from *Cp* mutants,[27−29,31,34,38,46,55] it was suggested that these selected residues influence the Rd redox potential (see also, next section). The correlation of measured and calculated Rd redox potentials of all 15 Rd's yields now an RMSD of only 16 mV (open symbols in Figure 2; values listed in Supporting Information Table S7). This is a significant improvement compared to the results obtained by optimizing hydrogen atom positions only ("×" in Figure 2). For 13 of these Rd's, the redox potentials were measured, while for two Rd's (from WT *Ps* and from V44A/G45P mutant *Cp*; red right-facing △ in Figure 2), only estimated values are available. Nevertheless, no difference in quality of agreement with computed values could be observed for the latter two.

The largest discrepancies are systematic deviations that occur for redox potentials of the three Rd's from *Pa* (green △ in Figure 2). These were measured in the same lab[25,80] using polylysine as a redox mediator, which may have caused an upshift of the measured redox potential by about 20 mV.[91] The RMSD increases slightly (17 mV), if we consider the 12 Rd's where crystal structures are available only for the oxidized states (red right-facing △, green △, and magenta ▽ in Figure 2). It becomes smaller (8 mV), considering only the three Rd's (blue ◇ in Figure 2) where crystal structures are available for both redox states that were used to generate the RACs and where systematic deviations of the measured redox potentials (green △ in Figure 2) are excluded. Furthermore, we observe small but systematic deviations for the computed redox potentials to lower values for the Rd's where crystal structures are only available for the oxidized states (open triangles in Figure 2), while this seems to be not the case for the three redox potential values obtained for Rd's where crystal structures are available for both redox states (blue ◇ in Figure 2). In fact, it can be expected that the energy of a reduced state is higher if it is computed on the basis of the structure of the oxidized state, rendering computed redox potentials more negative as compared to the measured values. An analysis of the amide H-bond lengths reveals that they are slightly shorter (by less than 0.1 Å, Supporting Information Table S6) for the reduced state than for the oxidized state. Ignoring these small structural differences in the computation of Rd redox potentials may explain this small systematic deviation.

The relatively large differences in the sequences of the considered Rd's from seven different species make it difficult to

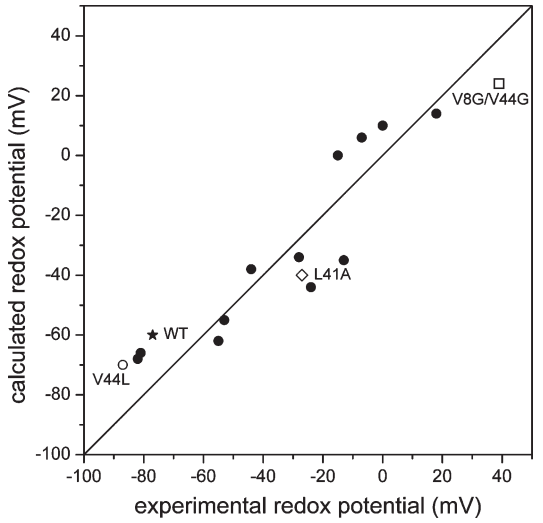

Figure 3. Comparison of 16 experimental and computed redox potentials of Rd's from WT and mutant *Cp*. Values presented in Supporting Information Table S8. On the basis of the Rd crystal structure from WT *Cp* (1IRO), the structures of 15 single and double mutants (V8A, V8D, V8G, V8I, V8L, V8R, V44A, V44G, V44I, V44L, V8G/V44G, V8I/V44G, V8I/V44I, V44A/G45P, and L41A) were modeled, and the redox potentials were computed (★, WT; ○, mutant V44L; ●, other mutants). For four mutants (V44L, V44A, V44G, and V44A/G45P), crystal structures are available. These were, however, not used to generate the RACs, except for mutant V44L, where a short side chain is exchanged by a long side chain. To reduce the number of necessary RACs, we used the rotamer of side chain L44 from the corresponding mutant crystal structure. Some mutants explicitly discussed in the text are labeled in the figure.

explain how individual amino acids may contribute to the shifts of redox potentials. Therefore, we will continue our study, focusing on the redox potentials of mutant Rd's from the same species. Nevertheless, a trend can be observed on the basis of the results presented so far: replacing small by large hydrophobic side chains in positions 8, 41, and 44 decreases the solvent accessibility of the FeS complex and consequently lowers its redox potential.[29]

3. Redox Potentials of Mutant Rd's Based on Crystal Structures from WT Cp. We tried to assess the structure−function relationship between mutated residues and the FeS complex redox potential. For this purpose, we used the crystal structure of oxidized Rd from WT *Cp* (1IRO) as a scaffold to construct structures of 15 Rd's from mutant *Cp* (mutated at sequence positions 8, 41, 44, and 45) for which the FeS complex redox potentials have been measured (Table S5, Supporting Information). We generated an extended set of RACs with optimized side chains in six sequence positions (5, 8, 41, 44, 45, and 48; see Figure 1) involving mutated residues and direct neighbors of the FeS complex as well as side chains involved in salt-bridge networks (D29-K31-D32, D35-K46, and E51-K2-E53). With this extended set of RACs, computed and measured Rd redox potentials yielded a surprisingly good agreement with measurements showing an RMSD of only 14 mV (Figure 3; values listed in Supporting Information Table S8). Again, this is a considerable improvement compared to the preceding results where the minimal set of RACs was used ("×" symbols in Figure 2).

The data set of the 15 Rd's from mutant *Cp* and the corresponding WT Rd are suitable to demonstrate how the Rd

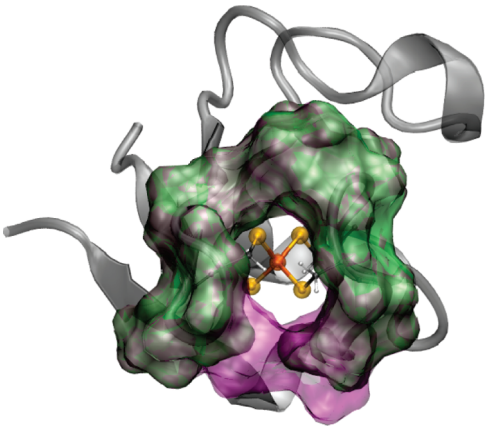

Figure 4. Comparison of solvent accessible surface for two Rd mutants from *Cp*: V8G/V44G (green) and V44L (purple). The replacement of Val in positions 8 and 44 with two Gly's in WT Rd from *Cp* exposes the FeS more to the solvent, while replacement with large amino acids like Leu isolates the FeS complex from the solvent. Rd's with a more solvent exposed FeS complex possess a more stabilized reduced state, leading to an upshift of the redox potential.

redox potentials vary, if the protein dielectric constant ε_p is set to 2 and 8. But, we will continue to strictly stick to $\varepsilon_p = 4$, a value which we have found to be optimal and have used exclusively for more than 15 years. In both cases $\varepsilon_p = 2$ and 8, the results are very poor, yielding RMSDs of 37 and 38 mV using redox potential reference values of 173 and −18 mV, respectively (for more details, see Figure S1 of the Supporting Information).

Since the protein backbone atom coordinates were kept invariant in all of these modeled Rd structures, the H-bond geometries of the FeS complex involving only backbone amide groups did not vary with mutant Rd's and redox states. Hence, the variation of Rd redox potentials can be explained by other factors than the local H-bond geometry around the FeS complex. One such important factor seems to be the FeS complex solvent accessibility and its variations with the redox states. This is corroborated by the Rd crystal structures from WT[31,38] and L41A mutant *Cp*,[34] showing variations of T5, K31, I12, and L41 side chains (Supporting Information Figure S2). In the high resolution Rd crystal structure from WT *Cp* (PDB ID 1IRO), several residues (T5 P15, K31, L41, and E50) appear in multiple side chain conformations. Analog variations of residue side chains were also observed for Rd's from *Cp* mutants (Supporting Information Table S4).

The WT Rd from *Cp* possesses, at −77 mV, one of the lowest measured Rd redox potentials (★ in Figure 3). The largest Rd redox potential of +39 mV was obtained for the double mutant V8G/V44G from *Cp* (□ in Figure 3), while the L41A mutant from *Cp* has a redox potential lying in the center of the interval of measured Rd redox potentials (−27 mV, ◇ in Figure 3). When the bulky residue Val is replaced with Gly, as done in the double mutant V8G/V44G from *Cp*, the FeS complex becomes more solvent exposed (see Figure 4). This stabilizes the reduced state (more negatively charged than the oxidized state) more than the oxidized state, resulting in an upshift of the Rd redox potential. Dependences of the Rd redox potential on sizes of amino acid side chains of Rd's from *Cp* in positions 8 and 44 were already identified for several Rd mutants.[27] Accordingly, small amino acids like Gly upshift the redox potential, while large amino acids like Leu downshift the redox potential.

The most populated RACs of the oxidized and reduced states contain multiple conformers of L41 (Supporting Information Figure S3). We observed that L41 is less buried in the reduced state and thus opens a small cavity near the FeS complex. This "open" L41 conformer correlates with results of MD simulations, where a water molecule near L41 gets closer to the FeS complex in the reduced state.[31,34] We forced the L41 side chain not to switch to the open conformer in the reduced state, which as expected downshifted the computed Rd redox potential by 34 mV. Alternative side chain rotamers for T5, T7, V8, I12, and Q48 were modeled showing only small variations of the Rd redox potential (about 10 mV), since these alternative conformations were only marginally populated in our RACs. Other multiple side chain conformers involving P15, K31, and E50 found in the Rd crystal structure from WT *Cp* (1IRO) had also practically no influence on the Rd redox potential.

The three salt bridges (K31-D29, K31-D32, and K46-D35, Supporting Information Table S3) present in the Rd crystal structure from WT *Cp* (1IRO) are also present in all RACs of Rd's from *Cp* mutants. Additional charged residues introduced in the mutants V8D and V8R do not form additional salt-bridges in the generated RACs. In both mutants, the redox potentials are upshifted compared to WT Rd (measured, 49 mV and 62 mV; computed, 26 mV and 58 mV, respectively). The upshift is surprising for the mutant V8D, since a negative charge (D8 was found to be deprotonated) is introduced, which is expected to stabilize the oxidized state of the FeS complex and, therefore, decrease its redox potential. Our computations can qualitatively explain this effect: Asp8 is solvent exposed and does not interact directly with the FeS complex that becomes more solvent exposed in this mutant, thus, upshifting the redox potential.

4. Differences between Rd's from Cp and Pf. Understanding redox potential variations between the Rd's from the mesophilic (*Cp*) and thermophilic (*Pf*) species has been the concern of many studies.[16,27,28,31−33,39,44,45,48,49,51,52,56,57,93] It has been suggested that the presence of A44 in Rd from *Pf* contributes significantly to an upshift of the Rd redox potential.[28] However, there are variations in the Rd sequences from *Cp* and *Pf* at 24 sequence positions that may influence the redox potential. Alternatively, it was inferred from NMR spectroscopy on Rd's of WT and several mutants from *Cp* that the strength of the six amide H bonds (characterized by lengths) with the FeS complex sulfurs may have a major influence on the Rd redox potentials.[15,23] Consequently, we compared the H-bond lengths of the crystal structures of the two Rd's from *Cp* and *Pf*. In fact, they are just slightly longer by about 0.07 (0.08) Å for the Rd from the mesophilic *Cp* as compared to the Rd from the thermophilic *Pf* in the corresponding oxidized (reduced) state (see Supporting Information Table S6). Hence, due to shorter amide H bonds, the reduced state is slightly more stabilized for the Rd from *Pf* than from *Cp*, yielding a redox potential that is higher for the former than for the latter Rd. Indeed, at room temperature, the measured Rd redox potential from *Pf* is 108 mV higher compared to the Rd from *Cp*. Hence, one might conclude that each of the six amide H bonds contributes on average a redox potential shift of 18 mV to make up the difference, which sounds reasonable. To verify this conclusion, we computed for each of the six amide H bonds the full contributions to the FeS complex redox potential by setting to zero the backbone charges of the corresponding NH and direct neighbor groups (C═O, C_αH). We observed upshifts of the Rd redox potentials of on average 60 mV (Supporting Information Table S9) due to individual amide H-bond formation for both proteins, in agreement with recent *ab initio* quantum chemical computations on FeS complex model complexes.[21] The computed upshifts of the redox potentials were per H bond on average nearly the same for both proteins: 61.5 mV and 65 mV for the Rd's from *Cp* and *Pf*, respectively (Supporting Information Table S9). Hence, according to our computations, only 21 mV of the redox potential difference between Rd's from *Cp* and *Pf* is due to the difference in the amide H bonds, and the preceding conclusion is wrong. Obviously, there are other sequence related factors (the sequences of Rd from *Cp* and *Pf* differ in 24 positions) in the environment of the H bonds influencing the redox potentials of the two Rd's, as we will show in the following. Note that the conclusion on the limited role of the amide H bonds for the preceding case is not necessarily in conflict with our suggestion that the temperature dependence of the Rd redox potential from *Pf* may very well be explained by increasing H-bond lengths at higher temperatures, since in the latter case no sequence variations can interfere.

Without considering the peptide terminal groups and the FeS complex itself, there are three positively and 13 negatively charged residues in the WT Rd from the mesophilic *Cp*, while in the WT Rd's of the thermophilic species from *Pf* and *Pa*, there are five and six positively and 13 and 13 negatively charged residues, respectively. In the crystal structures, only part of these charged residues are involved in salt bridges. In contrast, the RACs generated for the two thermophilic Rd's from *Pf* and *Pa* notably involve more salt bridges than the corresponding crystal structures (see Table S10, Supporting Information). But, we found that these additional salt bridges have in general only a small influence on the Rd redox potentials (albeit they may be important for thermostability; Table S11, Supporting Information), such that they cannot be used to explain the redox potential differences of the Rd's from *Cp* and *Pf*. By setting to zero the atomic partial charges of all charged side chains, we observed downshifts of redox potentials by −63 mV and −38 mV for the Rd's from *Cp* and *Pf*, respectively (Table S9 Supporting Information). Hence, the different composition in charged amino acids can account for about a 25 mV difference in Rd redox potentials. The contributions of the backbone conformers are around 45 mV more positive for *Pf* than for *Cp* (values where obtained by setting the charges of backbone atoms to zero and computing the resulting shift in redox potential, see also Table S9), from which less than the half (21 mV) is due to differences in H-bond strengths. Hence, we can explain explicitly (25 mV + 45 mV) 70 mV of the total difference of 108 mV between the redox potentials of Rd's from WT *Cp* and *Pf*, although the sum of these contributions is not strictly additive. The remaining difference in the two Rd redox potentials results from a larger number of small contributions which are due to subtle variations in solvent accessibility and charge distributions that can also involve small changes in protonation pattern.

5. Variation of the H-Bond Number in Mutant Rd's from Pa. The crystal structure of the mutant Rd (W4L/R5S) from *Pa* (1YK5) was solved at high resolution (∼0.7 Å) in the oxidized state. It exhibits multiple side chain conformers for six residues (five residues have two and one three conformers), which are not too distant to influence the FeS complex. In addition, the Rd crystal structure of the mutant shows for Lys7-Ile8-Cys9 two backbone conformations on which we will focus in our next modeling steps. One backbone conformation corresponds to the WT crystal structure from *Pa*; the second

backbone conformation differs from WT in the amide plane between Cys9−Ile8 that is rotated by about 20° and in the amide plane between Ile8−Lys7 that is translated by about 0.13 Å. We considered this protein backbone variation to understand how the amide H bond with the FeS complex can affect the Rd redox potential. In the Rd's from WT (W4L/R5S mutant) *Pa*, the amide H bonds formed by residues K7 and I8 exhibit N−S distances of 3.54 and 3.62 Å (3.41 and 3.79 Å), respectively. Hence, in the Rd from mutant *Pa*, one amide H bond is shorter and the other longer compared to the Rd from WT *Pa*.

For a careful case study on the influence of amide H-bond length variations, we modeled three different backbone conformations using side chain and backbone conformations of WT Rd from *Pa* except for (1) K7, (2) I8, and (3) both K7 and I8, where we used the backbone conformation of the W4L/R5S mutant Rd from *Pa* to change the corresponding amide H-bond lengths, while the torsion angles of the side chains of K7 and I8 were kept at the WT conformations. Finally, we also considered the Rd conformation (4), where we varied both amide H bonds and the side chain conformations of K7 and I8 simultaneously. Shortening of the amide H bond with K7 (case 1) yielded a redox potential upshift of 18 mV, while stretching the H bond (case 2) yielded a downshift by −21 mV. These shifts nearly cancel when varying both amide H bonds (case 3), yielding a small downshift of −7 mV. Interestingly, when also the side chain conformation was varied (case 4), a redox potential upshift of 23 mV was obtained. Thus, assuming no H-bond variation with the change in redox state, we could estimate (from cases 1 and 2) that shortening an amide H bond by 0.1 Å results in an upshift of about 13 mV. If all six amide H-bonds lengths would be stretched by about 0.1 Å and there would be no other structural variations as in the preceding case study, the small individual contributions to the Rd redox potential would add up to a relatively large downshift of about 65 mV, as we would expect for the Rd structures at higher temperatures. However, as seen from the comparison of the Rd's from *Cp* and *Pf* (see discussion in the preceding subsection 4), the influence of other sequence related factors may destroy correlations between H-bond strengths and redox potential shifts.

To investigate the influence of an S··· HO H bond on Rd redox potentials, Bönisch et al.[25] generated the Rd triple mutant W4L/R5S/A44S from *Pa* whose Ser44 OH group forms an additional H bond with Cys6 of the FeS complex, whose length is 3.24 Å. In contrast to the corresponding double mutant W4L/R5S, the triple mutant does not involve multiple backbone conformers at Cys9. Hence, the six amide H bonds with the FeS complex remain intact. The measured redox potential upshift of the Rd triple mutant relative to the double mutant is 56 ± 20 mV.[25] This value is similar to our computed upshift of 39 mV using the crystal structure of the Rd triple mutant W4L/R5S/A44S from *Pa* (see Table S7, Supporting Information). In the most occupied RACs, Ser44 forms predominantly a H bond with Cys6, in agreement with the crystal structure. However, there are also RACs where Ser44 forms a H bond with Cys42, which is also a ligand of the FeS complex.

Alternatively, using the crystal structure of the Rd double mutant W4L/R5S from *Pa*, we modeled the Rd triple mutant that includes an extra O−H···S H bond. In this Rd structure, only the Ser44 side chain was optimized, which allowed estimation of the effect from this additional H bond excluding other influences. The resulting redox potential upshift of 58 mV is in good agreement with previously computed values[21] and experimental estimates.[25]

CONCLUSIONS

Continuum electrostatic energy computations were applied on rubredoxin structures (RACs) generated from all information of available crystal structures to evaluate FeS complex redox potentials. The RACs are the result of limited geometry optimizations on the different crystal structures, performed self-consistently with a proper protonation pattern at a given pH and solvent redox potential. If only hydrogen atom positions were optimized self-consistently, the RMSD between measured and computed redox potentials of Rd's with 15 different sequences was 42 mV, while the measured redox potentials vary only between −86 mV and +31 mV. This poor result is enormously improved, if additional RACs were used that consider all combinations of optimized side chains for residues that are mutated or involved in salt bridges or close to the FeS complex, yielding an RMSD of only 16 mV.

Rd structures are generally very rigid. Therefore, Rd crystal structures can be at high resolution where they exhibit subtle structural variations like multioccupancies, which are used in the generated RAC structures. Using a larger number of such RACs, we can obtain higher accuracies. This is the main reason that we obtained for the computed Rd redox potentials better agreement with measured values. For molecular systems, whose structures are less well-defined, the agreement with measured redox potentials is generally of lower quality.

Although the composition of charged groups and formation of salt bridges differ considerably between the mesophilic Rd from *Cp* and the thermophilic Rd from *Pf* and are considered to be responsible for the difference in thermostability, the contributions of charged residues to the redox potential difference between the two Rd's is small (25 mV).

For 16 Rd's (WT and 15 mutants) from *Cp* where measured redox potentials are available, RACs were generated solely on the basis of the WT crystal structure not varying the backbone, but with appropriate side chain optimizations as mentioned before. In this case, the computed Rd redox potentials showed an RMSD with measured data of only 14 mV. In the RACs used for these computations, the amide H-bond lengths with the FeS complex did not vary. Hence, the excellent agreement between measured and computed redox potentials does not support the general assumption that mainly differences in amide H-bond strengths are responsible for variations in Rd redox potentials. This result is not in conflict with the experimentally observed correlation of H-bond strengths with Rd redox potentials. But, this correlation does not prove that the H-bond variation is the origin of the redox potential variations in different Rd's.

On the other hand, removing one of these amide H bonds downshifts the Rd redox potential by about 60 mV. Thus, the fact that Rd redox potentials are relatively high, lying in the interval −90 mV to +40 mV, is determined by the presence of the six amide H bonds. This was the basis to assume that the variation of the measured redox potentials in different Rd's (from different mutants and different species) should be mainly due to different H-bond strengths, where the latter are related to the H-bond lengths. These amide H-bond lengths vary in Rd crystal structures. However, when the crystal structures of WT Rd's from *Cp* and *Pf* are compared, it turns out that these H bonds are

just slightly shorter for the latter Rd and the corresponding influence on the Rd redox potential is as expected small.

We estimated that variation of an amide H-bond length by 0.1 Å can shift the Rd redox potential by 13 mV. But, this value cannot straightforwardly be used to understand the variations of redox potentials in different Rd's, since this estimate was obtained by considering that only the amide backbone atoms are varied. As we have demonstrated in the present study, such backbone changes typically go along with variations of amino acid side chains, resulting in a total shift of the redox potential, which may even go in the opposite direction.

In summary, the variations in redox potentials of different Rd's are not the result of a single factor but are due to combinations of backbone and side chain variations, which lead to subtle changes of the electrostatic boundary between the protein and solvent, rendering the FeS complex more or less solvent exposed. Furthermore, differences in composition of charged residues for Rd's from different species play some role, while variations in the salt-bridge pattern alone have no significant effect. Finally, the variation of amide H-bond strengths, which was traditionally considered to play a major role, has only a very moderate influence on the Rd redox potentials.

■ ASSOCIATED CONTENT

Supporting Information. Details of the methodology, a list of Rd PDB information, measured redox potentials and references, *Cp* mutant conformations obtained after structural alignment, and atomic partial charges as well as figures of conformations in crystal structures and RACs. This material is available free of charge via the Internet at http://pubs.acs.org.

■ AUTHOR INFORMATION

Corresponding Author

*Fax: +493083856921. E-mail: knapp@chemie.fu-berlin.de.

■ ACKNOWLEDGMENT

We thank Dr. Galstyan for useful discussions. This work was supported by Volkswagen Foundation, JST PRESTO program (H.I.); Grant-in-Aid (H.I. 21770163) for Science Research from the Ministry of Education, Science, Sport and Culture of Japan; Special Coordination Fund for Promoting Science and Technology of MEXT (H.I.); and Takeda Science Foundation (H.I.). A.P.G.H. and G.K. would like to thank CONACyT/DAAD and German National Academic Foundation for financial support.

■ ABBREVIATIONS

Cp, Clostridium pasterianum; *Dd, Desulfovibrio desulfuricans*; *Dg, Desulfovibrio gigas*; *Dv, Desulfovibrio vulgaris*; FeS complex, iron sulfur complex; MD, molecular dynamics; PB equation, Poisson−Boltzmann equation; PAC, pH adapted conformation; *Pa, Pyrococcus abyssi*; *Ps, Pseudomonas auruginosa,*; *Pf, Pyrococcus furiosus*; RAC, redox adapted conformation; RMSD, root-mean-square deviation; Rd, rubredoxin; WT, wild type

■ REFERENCES

(1) Hall, D. O.; Cammack, R.; Rao, K. K. *Origins Life Evol. Biosphere* **1974**, *5*, 363–386.
(2) Holm, R. H.; Kennepohl, P.; Solomon, E. I. *Chem. Rev.* **1996**, *96*, 2239–2314.
(3) Beinert, H.; Holm, R. H.; Münck, E. *Science* **1997**, *277*, 653–659.
(4) Imsande, J. *Plant Physiol. Biochem.* **1999**, *37*, 87–97.
(5) Beinert, H. *J. Biol. Inorg. Chem.* **2000**, *5*, 2–15.
(6) van Belien, J. B.; Neuenschwander, M.; Smits, T. H. M.; Roth, C.; Balada, S. B.; Witholt, B. *J. Bacteriol.* **2001**, *184*, 1722–1732.
(7) Hagelueken, G.; Wiehlmann, L.; Adams, T. M.; Kolmar, H.; Heinz, D. W.; Tümmler, B.; Schuber, W. D. *Proc. Natl. Acad. Sci. U. S. A.* **2007**, *104*, 12276–12281.
(8) Noodleman, L.; Norman, J. G., Jr.; Osborne, J. H.; Aizman, A.; Case, D. A. *J. Am. Chem. Soc.* **1985**, *107*, 3418–3426.
(9) Mouesca, J. M.; Chen, J. L.; Noodleman, L.; Bashford, D.; Case, D. A. *J. Am. Chem. Soc.* **1994**, *116*, 11898–11914.
(10) Noodleman, L.; Lovell, T.; Liu, T.; Himo, F.; Torres, R. A. *Curr. Opin. Chem. Biol.* **2002**, *6*, 259–273.
(11) Torres, R. A.; Lovell, T.; Noodleman, L.; Case, D. A. *J. Am. Chem. Soc.* **2003**, *125*, 1923–1936.
(12) Noodleman, L.; Han, W. G. *J. Biol. Inorg. Chem.* **2006**, *11* 674–694.
(13) Schreiner, E.; Nair, N. N.; Pollet, R.; Staemmler, V.; Marx, D. *P. Natl. Acad. Sci. U. S. A.* **2007**, *104*, 20725–20730.
(14) Solomon, E. I.; Xie, X.; Dey, A. *Chem. Soc. Rev.* **2008**, *37* 623–638.
(15) Lin, I. J.; Gebel, E. B.; Machonkin, T. E.; Westler, W. M.; Markley, J. L. *Proc. Natl. Acad. Sci. U. S. A.* **2005**, *102*, 14581–14586.
(16) Stephens, P. J.; Jollie, D. R.; Warshel, A. *Chem. Rev.* **1996**, *96*, 2491–2531.
(17) Hunsicker-Wang, L. M.; Heine, A.; Chen, Y.; Luna, E. P.; Todaro, T.; Fee, J. A. *Biochemistry* **2003**, *42*, 7303–7317.
(18) Venkateswara, R.; Holm, R. H. *Chem. Rev.* **2004**, *104*, 527–559.
(19) Gunner, M. R.; Mao, J.; Song, Y.; Kim, J. *Biochim. Biophys. Acta* **2006**, *1757*, 942–968.
(20) Dey, A.; Jenney, F. E., Jr.; Adams, M. W. W.; Babini, E.; Takahashi, Y.; Fukuyama, K.; Hodgson, K. O.; Hedman, B.; Solomon, E. I. *Science* **2007**, *318*, 1464–1468.
(21) Gamiz-Hernandez, A. P.; Galstyan, A. S.; Knapp, E. W. *J. Chem. Theory Comput.* **2009**, *5*, 2898–2908.
(22) Adman, E. T.; Watenpaugh, K. D.; Jensen, L. H. *Proc. Natl. Acad. Sci. U. S. A.* **1975**, *72*, 4854–4858.
(23) Lin, I. J.; Gebel, E. B.; Machonkin, T. E.; Westler, W. M.; Markley, J. L. *J. Am. Chem. Soc.* **2003**, *125*, 1464–1465.
(24) Solomon, E. I.; Gorelsky, S. I.; Dey, A. *J. Comput. Chem.* **2006**, *27*, 1415–1428.
(25) Bönisch, H.; Ladenstein, R. *J. Biol. Inorg. Chem.* **2007**, *12*, 1163–1171.
(26) Zheng, Q.; Smith, E. T.; Kurtz, D. M., Jr.; Scott, R. A. *Inorg. Chim. Acta* **1996**, *242*, 245–251.
(27) Zheng, H.; Kellog, S. J.; Erickson, A. E.; Dubauskie, N. A.; Smith, E. T. *J. Biol. Inorg. Chem.* **2003**, *8*, 12–18.
(28) Eidsness, M. K.; Burden, A. E.; Richie, K. A.; Kurtz, D. M.; Scott, R. A.; Smith, E. T.; Ichiye, T.; Beard, B.; Min, T.; Kang, C. *Biochemistry* **1999**, *38*, 14803–14809.
(29) Xiao, Z.; Maher, M. J.; Cross, M.; Bond, C. S.; Guss, J. M.; Wedd, A. G. *J. Biol. Inorg. Chem.* **2000**, *5*, 75–84.
(30) Kennepohl, P.; Solomon, E. I. *Inorg. Chem.* **2003**, *42*, 689–695.
(31) Min, T.; Ergenekan, C. E.; Eidsness, M. K.; Ichiye, T.; Kang, C. *Protein Sci.* **2001**, *10*, 613–621.
(32) Day, M. W.; Hsu, B. T.; Joshuator, L.; Park, J. B.; Zhou, Z. H.; Adams, M. W.; Rees, D. C. *Protein Sci.* **1992**, *1*, 1494–1507.
(33) Yelle, R. B.; Park, N.-S.; Ichiye, T. *Proteins* **1995**, *22*, 154–167.
(34) Park, I. Y.; Youn, B.; Harley, J. L.; Eidsness, M. K.; Smith, E.; Ichiye, T.; Kang, C. *J. Biol. Inorg. Chem.* **2004**, *9*, 423–428.
(35) Millar, M.; Lee, J. F.; O′Sullivan, T.; Koch, S. A.; Fikar, R. *Inorg. Chim. Acta* **1996**, *243*, 333–343.
(36) Ullmann, G. M.; Noodleman, L.; Case, D. A. *J. Biol. Inorg. Chem.* **2002**, *7*, 623–639.
(37) Siegbahn, P. E. M.; Himo, F. *J. Biol. Inorg. Chem.* **2009**, *14*, 643–651.

(38) Dauter, Z.; Wilson, K. S.; Sieker, L. C.; Moulis, J.-M.; Meyer, J. *Proc. Natl. Acad. Sci. U. S. A.* **1996**, *93*, 8836–8840.
(39) Gillès de Pélichy, L. D.; Smith, E. T. *Biochemistry* **1999**, *38*, 7874–7880.
(40) Xiao, L.; Honig, B. *J. Mol. Biol.* **1999**, *289*, 1435–1444.
(41) Pace, C. N. *Nat. Struct. Biol.* **2000**, *7*, 345–346.
(42) Perl, D.; Mueller, U.; Heinemann, U.; Schmid, F. X. *Nat. Struct. Biol.* **2000**, *7*, 380–383.
(43) Blake, P. R.; Park, J. B.; Bryant, F. O.; Aono, S.; Magnuson, J. K.; Eccleston, E.; Howard, J. B.; Summers, M. F.; Adams, M. W. W. *Biochemistry* **1991**, *30*, 10885–10895.
(44) Bradley, E. A.; Stewart, D. E.; Adams, M. W.; Wampler, J. E. *Protein Sci.* **1993**, *2* (4), 650–665.
(45) Swartz, P. D.; Ichiye, T. *Biochemistry* **1996**, *35*, 13772–13779.
(46) Zeng, Q.; Smith, E. T.; Kurtz, D. M., Jr.; Scott, R. A. *Inorg. Chim. Acta* **1996**, *242*, 245–251.
(47) Lazardis, T.; Lee, I.; Karplus, M. *Protein Sci.* **1997**, *6*, 2589–2605.
(48) Eidsness, M. K.; Richie, K. A.; Burden, A. E.; Kurtz, D. M. J.; Scott, R. A. *Biochemistry* **1997**, *36* (34), 10406–10413.
(49) Bau, R.; Rees, D. C.; Kurtz, D. M.; Scott, R. A.; Huang, H.; Adams, M. W.; Eidsness, M. K. *J. Biol. Inorg. Chem.* **1998**, *3*, 484–493.
(50) Bertini, I.; Kurtz, D. M., Jr.; Eidsness, M. K.; Liu, G.; Luchinat, C.; Rosato, A.; Scott, R. A. *J. Biol. Inorg. Chem.* **1998**, *3*, 401–410.
(51) Grottesi, A.; Ceruso, M.-A.; Colosimo, A.; Di Nola, A. *Proteins: Struct., Funct., Genet.* **2002**, *46*, 287–294.
(52) Bonomi, F.; Burden, A. E.; Eidsness, M. K.; Fessas, D.; Iametti, S.; Kurtz, D. M. J.; Mazzini, S.; Scott, R. A.; Zeng, Q. *J. Biol. Inorg. Chem.* **2002**, *7*, 427–436.
(53) Bougault, C. M.; Eidsness, M. K.; Prestegard, J. H. *Biochemistry* **2003**, *42*, 4357–4372.
(54) Dolan, E. A.; Yelle, R. B.; Beck, B. W.; Fischer, J. T.; Ichiye, T. *Biophys. J.* **2004**, *86*, 2030–2036.
(55) Park, I. Y.; Eidsness, M. K.; Lin, I. J.; Gebel, E. B.; Youn, B.; Harley, J. L.; Machonkin, E. E.; Frederick, R. O.; Markley, J. L.; Smith, E. T.; Ichiye, T.; Kang, C. *Proteins* **2004**, *57*, 618–625.
(56) Bonomi, F.; Eidsness, M. K.; Iametti, S.; Kurtz, D. M. J.; Mazzini, S.; Morleo, A. *J. Biol. Inorg. Chem.* **2004**, *9* (3), 297–306.
(57) Sulpizi, M.; Raugei, S.; Vondele, J. V.; Carloni, P.; Sprik, M. *J. Phys. Chem. B* **2007**, *111*, 3969–3976.
(58) *CRC Handbook of Chemistry and Physics*, 84th ed; Press, C., Ed.; CRC Press: Boca Raton, FL, 1992.
(59) Rabenstein, B.; Ullmann, G. M.; Knapp, E. W. *Eur. Biophys. J.* **1998**, *27*, 626–637.
(60) Ullmann, G. M.; Knapp, E. W. *Eur. Biophys. J.* **1999**, *28*, 533–551.
(61) Rabenstein, B.; Knapp, E. W. *Biophys. J.* **2001**, *80*, 1141–1150.
(62) Popovic, D. M.; Zaric, S. D.; Rabenstein, B.; Knapp, E. W. *J. Am. Chem. Soc.* **2001**, *123*, 6040–6053.
(63) Voigt, P.; Knapp, E. W. *J. Biol. Chem.* **2003**, *278*, 51993–52001.
(64) Ishikita, H.; Morra, G.; Knapp, E. W. *Biochemistry* **2003**, *42*, 3882–3892.
(65) Ishikita, H.; Knapp, E. W. *J. Am. Chem. Soc.* **2004**, *126*, 8059–8064.
(66) Ishikita, H.; Knapp, E. W. *FEBS Lett.* **2005**, *579*, 3190–3194.
(67) Ishikita, H.; Knapp, E. W. *J. Am. Chem. Soc.* **2005**, *127*, 14714–14720.
(68) Ishikita, H.; Saenger, W.; Biesiadka, J.; Loll, B.; Knapp, E. W. *Proc. Natl. Acad. Sci. U. S. A.* **2006**, *103*, 9855–9860.
(69) Gamiz-Hernandez, A. P.; Kieseritzky, G.; Demir-Kavuk, O.; Galstyan, A. S.; Knapp, E. W. *ChemPhysChem* **2010**, *11*, 1196–1206.
(70) Schmidt am Busch, M.; Knapp, E. W. *J. Am. Chem. Soc.* **2005**, *127* (45), 15730–15737.
(71) Galstyan, A. S.; Knapp, E. W. *J. Comput. Chem.* **2009**, *30*, 203–211.
(72) Kieseritzky, G.; Knapp, E. W. *Proteins: Struct., Funct., Bioinf.* **2008**, *71*, 1335–1348.
(73) Kieseritzky, G.; Knapp, E. W. *J. Comput. Chem.* **2008**, *29* (15), 2575–2581.
(74) Holst, M.; Saied, F. *J. Comput. Chem.* **1993**, *14*, 105–113.
(75) Baker, N.; Sept, D.; Joseph, S.; Holst, M.; McCammon, J. *Proc. Natl. Acad. Sci. U. S. A.* **2001**, *98*, 10037–10041.
(76) Baptista, A. M.; Teixeira, V. H.; Soares, C. M. *J. Chem. Phys.* **2002**, *117*, 4184–4200.
(77) Lee, M. S.; F., R. S., Jr.; C., L. B., III. *Proteins: Struct., Funct., Bioinf.* **2004**, *56*, 738–752.
(78) Brooks, B. R.; Bruccoleri, R. E.; Olafson, B. D.; States, D. J.; Swaminathan, S.; Karplus, M. *J. Comput. Chem.* **1983**, *4*, 187–217.
(79) MacKerell, A. D., Jr.; Bashford, D.; Bellott, M.; Dunbrack, R. L., Jr.; Evanseck, J.; Field, M. J.; Fischer, S.; Gao, J.; Guo, H.; Ha, S.; Joseph, D.; Kuchnir, L.; Kuczera, K.; Lau, F. T. K.; Mattos, C.; Michnick, S.; Ngo, T.; Nguyen, D. T.; Prodhom, B.; Reiher, W. E., III; Roux, B.; Schlenkrich, M.; Smith, J.; Stote, R.; Straub, J.; Watanabe, M.; Wiorkiewicz-Kuczera, J.; Yin, D.; Karplus, M. *J. Phys. Chem B* **1998**, *102*, 3586–3616.
(80) Bönisch, H.; Schmidt, C. L.; Bianco, P.; Ladenstein, R. *Acta Crystallogr., Sect. D* **2005**, *61*, 990–1004.
(81) Watenpaugh, K. D.; Sieker, L. C.; Jensen, L. H. *J. Mol. Biol.* **1980**, *138*, 615–633.
(82) Sieker, L. C.; Stenkamp, R. E.; Jensen, L. H.; Prickril, B.; LeGall, J. *FEBS Lett.* **1986**, *208*, 73–76.
(83) Stenkamp, R. E.; Sieker, L. C.; Jensen, L. H. *Proteins* **1990**, *8*, 352–264.
(84) Frey, M.; Sieker, L.; Payan, F.; Haser, R.; Bruschi, M.; Pepe, G.; Legall, J. *J. Mol. Biol.* **1987**, *197*, 525–541.
(85) Chen, C. J.; Lin, Y. H.; Huang, Y. C.; Liu, M. Y. *Biochem. Biophys. Res. Commun.* **2006**, *349*, 79–90.
(86) Adman, E. T.; Sieker, L. C.; Jensen, L. H. *J. Mol. Biol.* **1991**, *217*, 337–352.
(87) Dauter, Z.; Sieker, L. C.; Wilson, K. S. *Acta Crystallogr., Sect. B* **1992**, *48*, 42–59.
(88) Misaki, S.; Morimoto, Y.; Ogata, M.; Yagi, T.; Higuchi, Y.; Yasuoka, N. *Acta Crystallogr., Sect. D* **1999**, *55*, 408–413.
(89) Kurihara, K.; Tanaka, I.; Chatake, T.; Adams, M. W. W.; Moiseeva, N.; Bau, R.; Niimura, N. *Proc. Natl. Acad. Sci. U. S. A.* **2004**, *101*, 11215–11220.
(90) Kabsch, W. *Acta Crystallogr., Sect. A* **1976**, *32*, 922–923.
(91) Xiao, Z.; Lavery, M. J.; Bond, A. M.; Wedd, A. G. *Electrochem. Commun.* **1999**, *1*, 309–314.
(92) Adams, M. W. *Adv. Inorg. Chem.* **1992**, *38*, 341–396.
(93) Swartz, P. D.; Beck, B. W.; Ichiye, T. *Biophys. J.* **1996**, *71*, 2958–2969.